Journal of Alloys and Compounds 913 (2022) 165281

Contents lists available at ScienceDirect

Journal of Alloys and Compounds

journal homepage: www.elsevier.com/locate/jalcom

Research Article

The unusual character of microstructure evolution during "abc" deformation of commercial-purity titanium

S. Mironov[a,*], S. Zherebtsov[a], S.L. Semiatin[b]

[a] Belgorod National Research University, Pobeda 85, Belgorod 308015, Russia
[b] Materials Resources LLC, Dayton, OH 45440, USA

ARTICLE INFO

Article history:
Received 23 February 2022
Received in revised form 19 April 2022
Accepted 29 April 2022
Available online 2 May 2022

Keywords:
Commercially-purity titanium
Severe plastic deformation
Ultrafine-grain materials
Electron backscatter diffraction (EBSD)
Microstructure

ABSTRACT

Microstructure evolution during "abc" deformation of commercial-purity titanium was investigated. Continuous dynamic recrystallization (CDRX) played a dominant role in the microstructural changes, although mechanical twinning also contributed to some extent. It was found that CDRX developed preferentially at the original grain boundaries, thus resulting in a necklace-type microstructure. This effect was attributed to the comparatively-high local stresses in these areas, which promoted pyramidal < c+a > slip and thus enhanced evolution of deformation-induced boundaries. It was also established that changes in strain path resulted in a noticeable re-organization of the pre-existing dislocation structure due to a Bauschinger Effect and thus promoted essential material softening. This phenomenon retarded the evolution of dislocation boundaries and thus tended to lead to stagnation in microstructure refinement.

1. Introduction

Due to its excellent biocompatibility, commercial-purity titanium (CP Ti) is very promising for biomedical applications [1]. Until recently, commercial usage of this material has been limited due to its comparatively-low mechanical strength. However, the development and implementation of severe plastic deformation (SPD) techniques has opened new opportunities for enhancing the mechanical properties CP Ti. In general, SPD approaches can impart considerable strengthening to metallic materials due to substantial refinements in grain size often in the ultrafine-grain (UFG) region [2–4].

Despite the benefits of SPD, only a few methods are feasible for the production of *bulk* UFG materials. One of these scalable methods, so-called "abc" deformation, involves sequential compression of a billet/workpiece along three orthogonal axes. In the literature, variants of this approach (sometimes involving a combination of upsetting and drawing) are also known as "multiple forging", "multi-axial forging", "multi-axial deformation", "multi-directional forging", etc. Because of its similarity to conventional open-die forging, "abc" deformation techniques are readily performed in industry. For example, the technique has been found to provide an efficient method for the production of UFG titanium [5–32].

The "abc" deformation of CP Ti has a number of distinctive features. First, to avoid excessive changes in shape during billet processing (and thus enable a virtually unlimited accumulation of strain), low-to-moderate reductions are usually imposed during each compression step (typically, ~40–50 pct.). To promote the grain-refinement effect and minimize cracking, processing is often conducted at a temperature between 400 and 500 °C (~0.35–0.40T_m, where T_m is the melting point). In other instances, "abc" deformation is applied at 200–350 °C (~0.24–0.32T_m) [6,18] or even ambient conditions [5,16–18]. In such cases, a relatively-low strain per pass (~10–25 pct.) is used [5,6].

At relatively-low accumulated strains, microstructure evolution in CP Ti typically involves extensive twinning [5,7,9,14,18,19,24,33]. The activation of twinning is usually attributed to the limited number of prism slip systems (i.e., the slip mode with the lowest critical resolved shear stress, or CRSS), which is insufficient to accommodate an arbitrary imposed strain; on the other hand, it is also promoted by the comparatively low CRSS for twinning [34].

Depending on the temperature of "abc" deformation, the activation of various twinning systems has been observed. At elevated temperatures, these include $\{10\bar{1}1\}$, $\{10\bar{1}2\}$, and $\{11\bar{2}3\}$ twinning [7]. At low temperatures, the operation of $\{11\bar{2}2\}$ and $\{10\bar{1}2\}$ twinning has been found; at times, secondary $\{11\bar{2}2\} \rightarrow \{10\bar{1}2\}$ twinning has also been reported [18].

After moderate strains, twinning is usually found to cease [7,18]. In addition, due to the influence of continuing strain, twin boundaries typically deviate from the exact twin-matrix orientation

* Corresponding author.
E-mail address: mironov@bsu.edu.ru (S. Mironov).

https://doi.org/10.1016/j.jallcom.2022.165281
0925-8388/

relationship and gradually transform into random (non-twin) grain boundaries [7,14,24,33]. Nevertheless, a small fraction of twins is sometimes noted even in heavily-deformed material [7]. Such observations are sometimes attributed to changes in strain path [7]. At high strains, microstructure refinement via continuous dynamic recrystallization (i.e., a mechanism involving the gradual transformation of subgrains into grains) is often reported [7–9,14,19,24,33]. As is normally expected in such instances, the heavily-deformed material often contains a significant portion of coarse-grain remnants [7,8,11,13,19], as well as a substantial percentage (up to ~30 pct.) of low-angle boundaries [7,13,19].

Although the scientific literature provides valuable insight into broad aspects of microstructure changes during "abc" deformation of CP Ti, some important aspects of this process are still unclear. Specifically, the detailed effect of changes in strain path on microstructure development remains poorly understood. For instance, it might be hypothesized that "abc" deformation would suppress crystallographic rotations of grains toward stable-end orientations, and thus enhance grain subdivision. Moreover, changes in strain path may result in shear banding [5,8,9,11,14] and twinning [7]. Taken together, these factors should enhance grain refinement compared with monotonic SPD techniques. To the present, however, such effects have *not* been observed experimentally. The present research was undertaken to clarify these issues, therefore.

2. Material and experimental procedures

The material used in the present investigation was CP Ti grade VT1–0 (per its Russian designation) with a nominal chemical composition shown in Table 1. The material was received as a hot-rolled bar with an equiaxed microstructure (supplementary Fig. S1). From the supplied bar, rectangular specimens measuring 16 × 18 × 20 mm^3 were machined parallel to the bar axis. These samples were subjected to "abc" deformation in air at 400 °C (≈0.35 T_m) and a nominal strain rate of 10^{-3} s^{-1}using a Schenk universal testing machine. The "abc" deformation involved 12 successive compression passes (~40 pct. height reduction each) along three orthogonal axes, as shown schematically in Fig. 1a. After each pass, the bulged surfaces of the compressed specimens were removed by electrical-discharge machining (EDM) to restore a rectangular shape. The accumulated strain was estimated as the sum of the true strains imposed during each of the passes.[1]

To establish microstructure evolution, observations were performed on specimens subjected to 1, 2, 3, 4, 7, and 12 passes. In addition, the condition developed during a single 15-pct. height reduction was also determined to quantify the initial stage of plastic flow and microstructure evolution. In all cases, microstructure observations focused on the central (most-heavily-deformed) location of each sample, and were conducted by electron backscatter diffraction (EBSD) and transmission electron microscopy (TEM).

For the EBSD measurements, deformed specimens were sectioned axially along the last compression. A suitable surface finish was obtained by mechanical grinding and polishing using conventional methods followed by final electro-polishing employing a solution of 80-pct. acetic anhydride + 20-pct. perchloric acid (chilled to ~10 °C) and an applied potential of 60 V.[2] EBSD was conducted using an FEI Quanta 600 field-emission-gun scanning-electron microscope (FEG SEM) equipped with a TSL OIM™ system and operated at an accelerating voltage of 30 kV. Depending on the particular material condition, the EBSD scan step size was varied from 0.2 to 0.075 μm. To improve the fidelity of EBSD data, grains comprising three or fewer pixels were automatically removed ("cleaned") from EBSD maps using the standard grain-dilation option of the TSL software. Considering the angular accuracy of EBSD, misorientations below 2° were excluded from consideration. A 15° criterion was applied to differentiate low-angle boundaries (LABs) from high-angle boundaries (HABs). The grain size was measured using the circle-equivalent-diameter approach [35].

Samples for TEM foils were cut using EDM, ground using wet abrasive papers to a thickness of ~0.1 mm, and then jet-polished in a solution containing 5-pct. perchloric acid, 35-pct. butanol, and 60-pct. methanol at −30 °C. Microstructure observations were performed using a JEOL JEM 2100 TEM operated at 200 kV. Dislocation densities were measured using the linear-intercept approach.

Table 1
Nominal chemical composition of program material (wt pct.).

Ti	Fe	Si	O	C	N	H
Balance	≤ 0.25	≤ 0.10	≤ 0.20	≤ 0.07	≤ 0.04	≤ 0.01

3. Results

3.1. Broad aspects of microstructure changes

One of the major benefits of "abc" deformation is the ability to track material behavior using plots of flow stress as a function of cumulative strain, an example of which is shown in Fig. 1b.

In agreement with other results in the scientific literature [9,11,12,14,19], the initial deformation stage (i.e., the first three or four deformation passes) was characterized by marked strain hardening, which resulted in a nearly threefold increase in flow stress (Fig. 1b). Subsequent deformation, however, led to a saturation of the flow stress, and the material exhibited essentially a steady-state behavior thereafter. The latter effect is usually attributed to a balance between strain hardening and dynamic recovery, as well as the achievement of a steady-state microstructure [e.g., 36].

Another interesting observation was the substantial softening associated with each change of strain path, i.e., a decrease in flow stress during reloading relative to that at the end of the previous pass (Fig. 1b). This phenomenon was sometimes coupled with a Luders-like behavior after yielding (e.g., the third pass in Fig. 1b). The possible origin of this effect is discussed in Section 4.2.

3.2. Microstructure morphology and grain-size evolution

Taken from the central location of compressed specimens, EBSD inverse-pole-figure (ipf) maps for the final compression direction, including color-coded LABs and HABs (Fig. 2), and associated grain-size statistics (Fig. 3) indicated various trends as a function of cumulative strain.

3.2.1. Low strains

The most striking feature of microstructure evolution at low strain was extensive mechanical twinning (Fig. 2a). Assuming a specific misorientation across the twin boundaries (discussed in Section 3.3), the dominant twin modes included $\{10\bar{1}2\} < \bar{1}011>$, $\{10\bar{1}1\} < \bar{1}012>$, and $\{11\bar{2}3\} < \bar{1}\bar{1}22>$. The $\{10\bar{1}2\}$ and twins typically had a lenticular morphology and often extended across almost entire grains. In contrast, $\{11\bar{2}3\}$ twins were usually relatively fine in size. Occasionally, multiple as well as secondary twins were also observed. Equally important, the spatial distribution of the twins was not uniform, and a significant fraction of grains contained no twins. In the literature, this effect is sometimes attributed to specific

[1] Considering the preferential strain concentration in the center of a deformed specimen (intrinsic to compression tests), it was likely that the actual total strain was somewhat larger than that calculated based on the uniform-deformation assumption.
[2] This voltage is very high for electro-polishing of heavily-deformed material. Hence, future work to optimize its level is certainly warranted.

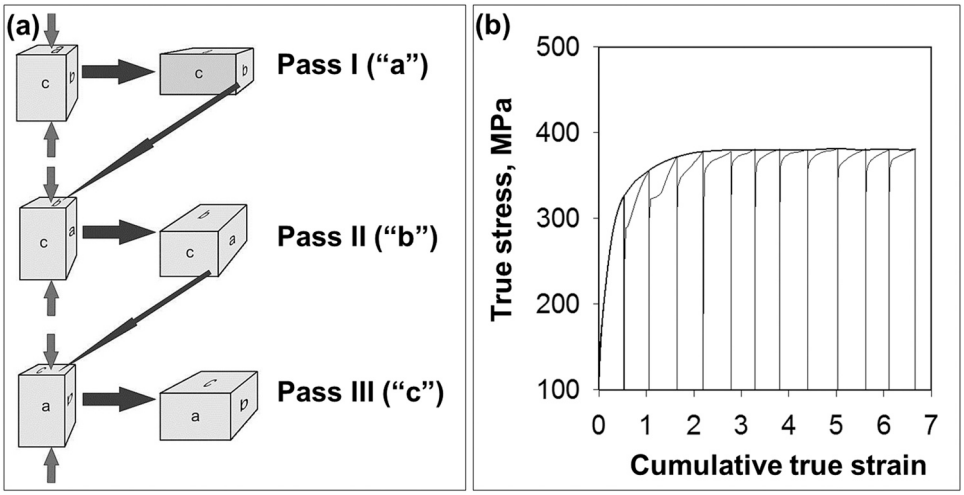

Fig. 1. (a) Schematic illustration of "abc" deformation and (b) a typical plot of true stress versus total (accumulated) strain.

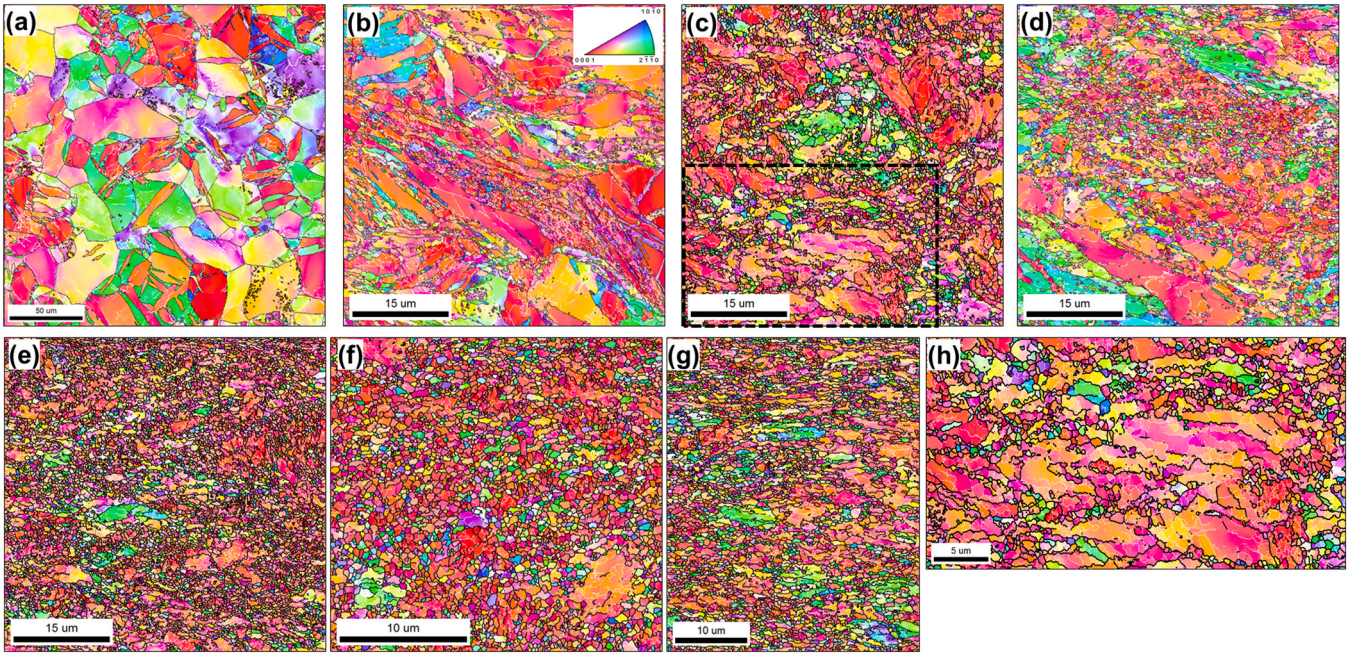

Fig. 2. EBSD inverse pole-figure maps showing microstructures developed in the central location of billets after a true strain of: (a) 0.16, (b) ~0.5 (1 deformation pass), (c) ~1.1 (2 passes), (d) ~1.6 (3 passes), (e) ~2.2 (4 passes), (f) ~3.8 (7 passes), (g) ~6.7 (12 passes), and (h) high-magnification image of the selected area shown in (c). In the maps, grains are colored relative to the last compression direction, and LABs and HABs are depicted as white and black lines, respectively. In all cases, the last compression axis is vertical. Note the difference in scale markers.

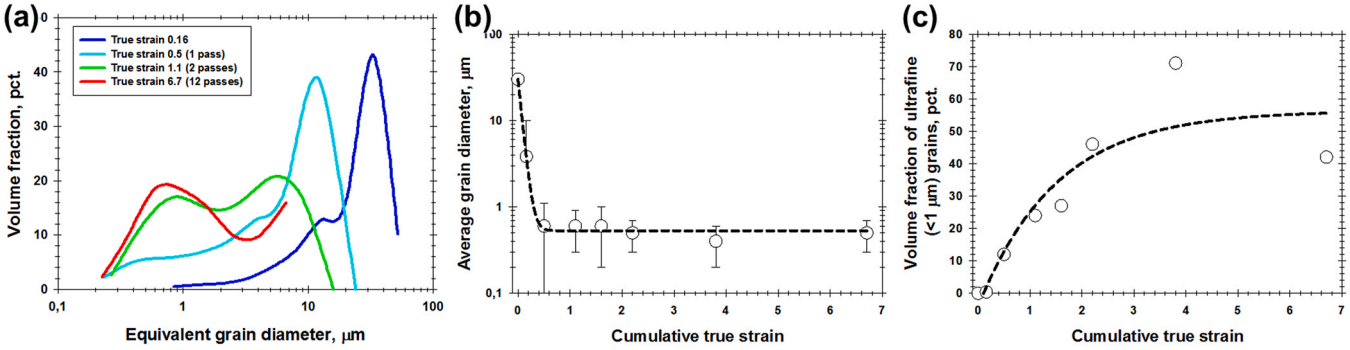

Fig. 3. Effect of "abc" deformation on (a) grain size distribution, (b) mean grain size, and (c) volume fraction of ultrafine (< 1 μm) grains. In (b), error bars show standard deviation.

crystallographic orientations of the twin-free grains which are more favorable for slip on prism systems < a > systems [e.g., 37].

The extensive twinning provided very marked and rapid grain refinement (Fig. 3a and b). Due to the heterogeneous character of the twinning process, however, microstructure refinement was not uniform. Specifically, the grain-size distribution tended to became somewhat bimodal (Fig. 3a).

The extensive development of LABs was also evident in the ipf maps (Fig. 2a). Typically, the LABs were found to cluster near original grain boundaries or within twins (Fig. 2a).

3.2.2. Large strains

An increase in the cumulative compression strain to ~0.5 (one pass) led to a flattening of the original grains as well as to the formation of new, relatively-fine grains (Fig. 2b). Both of these effects resulted in a shift of the grain-size distribution toward the finer range (Fig. 3a). Unexpectedly, the freshly-nucleated fine grains were often found to have a twin relationship with the surrounding matrix, and thus originated perhaps from twinning per se. It is also interesting to note that the mean grain size was measured to be ~0.6 μm (Fig. 3b), but the resulting microstructure did not appear to be ultrafine-grain in nature overall (Fig. 2b).

The second "abc" pass (total true strain ≈ 1.1) resulted in a marked enhancement in grain refinement (Fig. 2c). Nevertheless, the ultra-fine grains were distributed inhomogeneously throughout the material, tending to cluster near original grain boundaries or within twins (Fig. 2c). Hence, the microstructure became distinctly bimodal (Figs. 2c and 3a).

Additional increases in accumulated strain did not change the microstructure morphology noticeably. Instead, microstructure evolution was characterized principally by a gradual increase in the volume fraction of ultrafine grains (Figs. 2c-g and 3a). Furthermore, the *average* grain size experienced almost no change in this deformation range (Fig. 3b). For this reason, the volume fraction of ultrafine grains was measured as a function of cumulative strain to gain insight into the grain-refinement process (Fig. 3c).[3] At true strains below ~2.5, it was found to increase rapidly to a level of ~50 pct. At higher strains, the fine-grain fraction appeared to saturate, thus presumably reflecting the development of a stable microstructure that had also been inferred from the steady-state flow stress noted at these levels of deformation (Fig. 1b).

The origin of the ultrafine grains was of particular interest. A close inspection of the EBSD ipf maps (in particular the finer step-size scan in Fig. 2h) demonstrated that the surviving remnants of the parent grains contained a well-developed subgrain structure. In terms of morphology and characteristic size, the subgrains were broadly similar to the ultrafine grains. This presumably indicated that the latter originated from a gradual subgrain-to-grain transformation, i.e., via a continuous-dynamic-recrystallization mechanism. In this context, the distinctly-inhomogeneous distribution of ultrafine grains (Fig. 2c–g) was presumably associated with the preferential occurrence of this recrystallization mechanism at and near grain-boundary regions as well as within mechanical twins.

3.3. Misorientation distributions

Because grain refinement was governed by the development of deformation-induced boundaries, additional insight into microstructure development was garnered from plots of misorientation angle (Fig. 4a) and misorientation axis (Fig. 5) constructed from the EBSD data. The misorientation-angle data (Fig. 4a) were also expressed in terms of grain-boundary density, i.e., boundary length divided by the area of the EBSD map. These additional grain-boundary statistics are summarized in Fig. 4b-c and Table 2.

3.3.1. Low-to-moderate strains

As is normally expected for uniaxial compression, the height reduction to 40 pct. (true strain ≈ 0.5) resulted in substantial flattening of the original grains. This naturally enlarged the grain-boundary area seen in the longitudinal sections examined in the present work, and thus provided a measurable increase in grain-boundary density over the entire range of HABs from 15 to ~90° (Fig. 4a). As expected, a noticeable increase in LAB density was also found (Fig. 4a). These observations implied considerable slip activity. Hence, the misorientation axes of the low-angle (*dislocation*) boundaries were carefully analyzed (Fig. 5a–e). In this regard, the activation of a particular slip system rotates the crystal around the axis $\bar{w}//\bar{b}\times\bar{n}$, where $\bar{b}$ is the Burgers vector and $\bar{n}$ is the slip-plane normal. The relationships between the various slip systems in α (hcp) titanium and the corresponding rotation axes are summarized in Table 3 and Fig. 5f.

In view of the above considerations, the clustering of LAB axes near <0001> and <6$\bar{1}\bar{5}$3> poles found in the present work (Fig. 5a, b) indicated a prevalence of prism < a > and pyramidal < c+a > slip modes [38] (Table 3). The occurrence of prism slip with its low critical resolved shear stress (CRSS) is as expected. On the other hand, the activation of the pyramidal < c+a > slip mode was somewhat unexpected in view of its comparatively-higher CRSS.

The misorientation-angle/axis measurements for low-to-moderate strains (Fig. 5a, b) added credence to the activation of mechanical twinning as well. Specifically, the crystallographic preference of85^0 < 2$\bar{1}\bar{1}$0>, 57^0 < 2$\bar{1}\bar{1}$0>, and 87^0 < 10$\bar{1}$0> misorientations evidenced the activation of the {10$\bar{1}$2}, {10$\bar{1}$1}, and {11$\bar{2}$3} twinning modes, respectively (Table 2). In particular, these systems provided dense clusters near <2$\bar{1}\bar{1}$0> and <10$\bar{1}$0> poles in the misorientation-axis plots (Fig. 5a and b). Moreover, increased fractions of 28^o < 2$\bar{1}\bar{1}$0>, 38^o < 2$\bar{1}\bar{1}$0>, and 92^o < 16; $\bar{4}$; 12; 3> misorientations indicated the occurrence of secondary twinning via {10$\bar{1}$2} → {10$\bar{1}$1} and {10$\bar{1}$2} → {11$\bar{2}$3} (Table 2).

3.3.2. Large strains

An increase in cumulative true strain above ~0.5 promoted a gradual shift of the low-angle peak in the misorientation-angle distribution toward higher angles (Fig. 4a). This implied a gradual accumulation of misorientation across dislocation boundaries, thus providing further evidence of the activation of continuous dynamic recrystallization, as discussed in Section 3.2.2. Moreover, the HAB fraction of the misorientation distribution increased with strain initially, but then tended to saturate at value of ~60 pct. (Fig. 4b).

A preferential clustering of LAB axes near the <0001> and <6$\bar{1}\bar{5}$3>poles indicated a dominance of prism < a > and pyramidal < c +a > slip modes over the entire range of strain (Fig. 5c–e). By contrast, the fraction of twin-induced misorientations decreased rapidly to a nearly-random level (Table 2). Despite this decay, a surprisingly-high fraction was observed even after 3rd deformation pass (Table 2), which may have been associated with the re-activation of twinning due to the change in strain path per se.

The overall decrease in twin misorientaions with strain likely reflected a suppression of twinning in the high-strain rage as well as the gradual transformation of the original twin boundaries into random (non-twin-related) boundaries [7,14,18]. As a result, the twin-induced peaks disappeared almost completely from the misorientation distributions (Fig. 5c–e). Nevertheless, a small (but measurable) fraction of secondary {10$\bar{1}$2} → {11$\bar{2}$3} twins was still observed over the entire deformation range (Table 2), thus supporting the conclusion that some twinning, albeit subtle, was still possible even in heavily-deformed material.

[3] The significant experimental scatter in Fig. 3c is thought to be associated with the relatively-inhomogeneous microstructure distribution developed within compressed specimens.

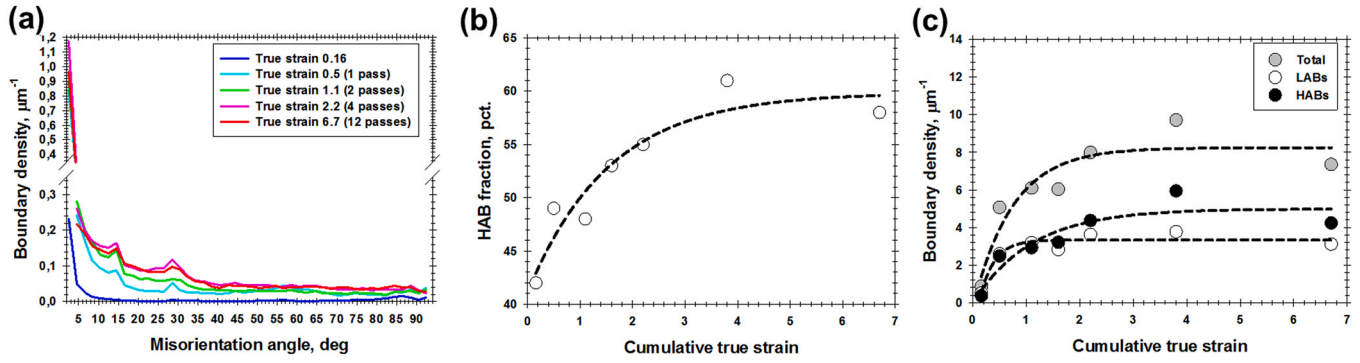

Fig. 4. Effect of "abc" deformation on (a) misorientation-angle distribution, (b) HAB fraction, and (c) grain-boundary density.

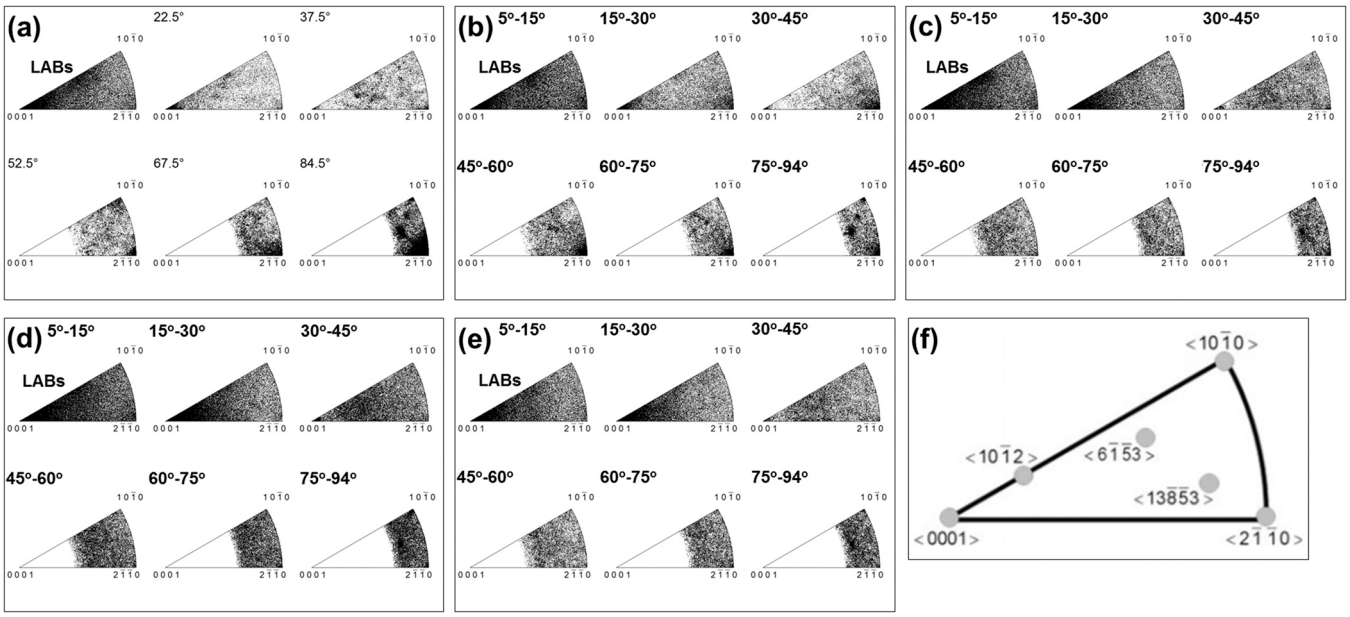

Fig. 5. Effect of cumulative true strain on misorientation-axis distribution: (a) 0.16, (b) ≈ 0.5 (1 deformation pass), (c) ≈ 1.1 (2 passes), (d) ≈ 2.2 (4 passes), (e) ≈ 6.7 (12 passes), and (f) standard unit triangle showing the Taylor axes of the slip systems available in a titanium (after Chun et al. [38]).

The grain-boundary density as a function of accumulated strain (Fig. 4c) provided an additional metric to quantify the microstructure-evolution process. At true strains below ~2, there was a major increase in total grain-boundary area. This observation was in line with the observed rapid grain refinement (Fig. 3c) and pronounced strain hardening (Fig. 1b) within this interval of deformation. At larger strains, however, grain-boundary evolution tended to cease, and even LAB-to-HAB transformation occurred to a very limited extent. This phenomenon thus explains the saturation of the grain-refinement process (Fig. 3b-c) and agreed well with the steady-state character of plastic flow (Fig. 1b). These phenomena are discussed in Section 4.2.

3.4. TEM observations

TEM observations provided more in-depth insight into microstructure evolution during "abc" deformation. TEM micrographs taken after different amounts of strain are summarized in Figs. 6 and 7; dislocation-density measurements are shown in Fig. 8.

3.4.1. Low-to-moderate strains

In specimens compressed to a 15-pct. height reduction, TEM observations confirmed the pronounced activity of mechanical twinning (Fig. 6a–c). Specifically, numerous examples of secondary twinning (indicated by the arrow in Fig. 6a), multiple twinning (Fig. 6b), and even strain-induced transformation of twins (arrow in Fig. 6c) were found. In addition, the extensive formation of dislocation boundaries and their arrangement into regular arrays were also observed (Fig. 6d).

After a true strain of ~0.5, an abrupt increase in dislocation density was observed (Fig. 8). As a result, the dislocation boundaries became the dominant microstructural feature (Fig. 6e). Quite noticeably, the boundaries were often found to be grouped in nearly-parallel series (Fig. 6e) thus showing some evidence of a lamellar-type structure, which is typical for heavily-deformed cubic metals [39]. Equally important, the density of sub-boundaries within grains varied noticeably (Fig. 6e and f), thus likely reflecting the non-uniform character of the strain distribution. It also appeared that the extensive formation of transverse boundaries tended to transform the lamellar structures into nearly-equiaxed ones (Fig. 6e and f).

3.4.2. Large strains

After reaching a cumulative true strain of ~2, the measured dislocation density tended to saturate (Fig. 7), thus mirroring the evolution of material strength (Fig. 1b) and trends in grain refinement (Figs. 3c and 4b-c). At this stage, the nearly-equiaxed dislocation substructure remained stable, experiencing insignificant changes in both morphology and scale (e.g., compare Fig. 7a and b). Broadly similar to

Table 2
Effect of accumulated strain on twin boundary fraction.

Twin mode	Misorientation	Area fraction of twin boundaries (within 5° tolerance), pct.						
		True strain ≈ 0.16	True strain ≈ 0.5 (1 pass)	True strain ≈ 1.1 (2 passes)	True strain ≈ 1.6 (3 passes)	True strain ≈ 2.2 (4 passes)	True strain ≈ 3.8 (7 passes)	True strain ≈ 6.7 (12 passes)
$\{11\bar{2}2\}<\bar{1}\,\bar{1}23>$	$64.62^o<10\bar{1}0>$	0.0	0.1	0.1	0.3	0.1	0.1	0.1
$\{11\bar{2}1\}<\bar{1}\,\bar{1}26>$	$35.10^o<10\bar{1}0>$	0.0	0.1	0.2	0.2	0.2	0.2	0.2
$\{10\bar{1}2\}<\bar{1}011>$	$84.78^o<2\bar{1}\,\bar{1}0>$	6.0	1.3	0.4	2.0	0.2	0.2	0.2
$\{10\bar{1}1\}<\bar{1}012>$	$57.42^o<2\bar{1}\,\bar{1}0>$	1.1	2.3	0.2	0.3	0.1	0.2	0.1
$\{\bar{1}\,\bar{1}24\}<\bar{2}\bar{2}43>$	$76.66^o<10\bar{1}0>$	0.0	0.0	0.1	0.1	0.1	0.1	0.1
$\{11\bar{2}3\}<\bar{1}\,\bar{1}22>$	$86.98^o<10\bar{1}0>$	1.0	0.5	0.2	0.5	0.4	0.2	0.1
$\{10\bar{1}2\}\rightarrow\{10\bar{1}1\}$ Secondary twinning	$28^o<2\bar{1}\,\bar{1}0>$	0.1	0.8	0.4	0.3	0.2	0.3	0.3
	$38^o<2\bar{1}\,\bar{1}0>$	0.0	0.6	0.2	0.2	0.2	0.2	0.2
$\{10\bar{1}2\}\rightarrow\{11\bar{2}3\}$ Secondary twinning	$92^o<16;\bar{4};12;3>$	1.3	1.2	0.8	1.3	0.5	0.5	0.7

Note: Boundary fractions ≥ 0.5 pct. are highlighted in gray.

Table 3
Relationship between slip mode and rotation axis (after Chun et al. [38]).

Slip mode		Rotation axis
Prism	$\{\bar{1}0\bar{1}0\}<2\bar{1}\bar{1}0>$	<0001>
Basal	$(0002)<2\bar{1}\bar{1}0>$	$<10\bar{1}0>$
Pyramidal <a>	$\{\bar{1}0\bar{1}1\}<2\bar{1}\bar{1}0>$	$<10\bar{1}2>$
Pyramidal I <c+a>	$\{\bar{1}0\bar{1}1\}<11\bar{2}3>$	$<13;\bar{8};\bar{5};3>$
Pyramidal II <c+a>	$\{11\bar{2}1\}<11\bar{2}3>$	$<6\bar{1}\bar{5}3>$

EBSD, TEM observations also revealed the relatively coarse-grained remnants in the heavily-deformed microstructure (Fig. 7c). However, it is important to note that the scale of the microstructures seen in TEM micrographs (Fig. 7a-b) was somewhat finer than that detected by EBSD (~0.2–0.3 μm vs ~0.5–0.6 μm). This finding implies that a significant portion of the deformation-induced boundaries likely had misorientations below the EBSD resolution limit and appeared to comprise a purely tangled-dislocation structure.

Of particular importance was the observation that the microstructures developed during sequential deformation passes were always aligned in a single common direction (e.g. Fig. 6e-f, and 7b). This direction was presumably associated with a particular orientation of the final compression axis. On the other hand, almost no evidence of microstructure alignment associated with the *previous* deformation pass (i.e., aligned in other directions) was found. The possible origin of such realignment is discussed in Section 4.2.

Despite the fact that the heavily-deformed microstructures were dominated by dislocation-induced boundaries, twin remnants were also observed sporadically (shown by the arrow in Fig. 7d). Moreover, apparently-fresh twins were also detected sometimes (arrow in Fig. 7e). As inferred from SEM EBSD, these TEM findings also suggested that mechanical twinning was not suppressed completely but occurred occasionally over the entire range of strains investigated in the present work. This observation agreed well with some reports in scientific literature [e.g. 40,41]. Nevertheless, it seems unlikely that this mechanism played a significant role in microstructure evolution at large strains.

In line with conclusions from SEM-EBSD analysis, TEM also failed to reveal any evidence of *discontinuous* dynamic recrystallization, or DDRX (which is typically characterized by thermal-activated grain-boundary bulging, the presence of recrystallization nuclei, etc.). Also in support of this finding, the dislocation densities appeared to be extremely high over almost the entire range of strains (Fig. 8). Therefore, it was highly unlikely that DDRX contributed to microstructure evolution.

The absence of dynamic restoration processes such as DDRX in CP Ti at the deformation temperature used in the present work (400 °C) is well known as being associated with the high mobility of interstitial (pinning) solutes (mainly oxygen, nitrogen, and carbon) that give rise to dynamic strain aging [34]. Despite the general TEM observations, however, sporadic dislocation-free grains were also observed (circled area in Fig. 7f).

4. Discussion

4.1. Specific character of continuous dynamic recrystallization in CP titanium

As shown in Sections 3.2 and 3.3, noticeable mechanical twinning in CP Ti had ceased after relatively-low strains. Therefore, the bulk UFG structure in this material originated mainly via continuous dynamic recrystallization (CDRX). CDRX in CP Ti exhibited some distinct differences relative to its occurrence in cubic metals, however. Specifically, CDRX in the present investigation was most pronounced near original grain (or twin-) boundaries, which eventually gave rise to a heterogeneous necklace-type microstructure (Fig. 2c–g). A similar effect has been also reported in several prior works [6,18]. The genesis of this phenomenon is considered in the present section.

It is well accepted that mechanical twinning normally results in marked strain hardening due partly to noticeable grain refinement and concomitant reductions in the mean free path of dislocations. In CP titanium, strain hardening is also due to the Basinski mechanism [42], in which formerly glissile matrix dislocations are “trapped” within twins and become sessile due to twin-induced crystallographic rotations [43]. In the present work, the overall strengthening effect was nearly threefold[4] (Fig. 1b). Such a large increase in

[4] Although the Basinski mechanism has been known for ~25 years, there is still no well-accepted approach to quantify its strengthening effect. Hence, the estimation of individual contributions to the overall material strength of grain refinement per se and the Basinski mechanism is challenging.

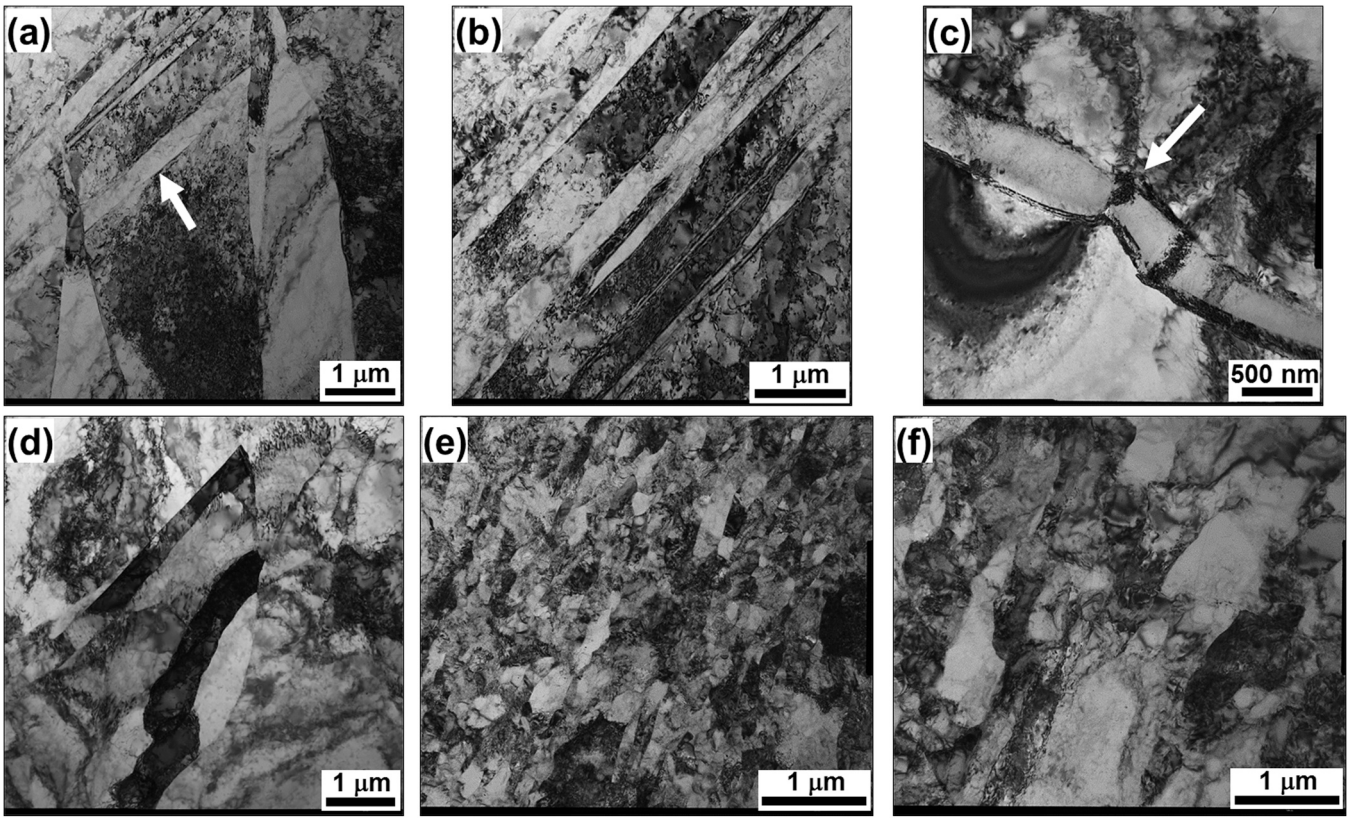

Fig. 6. TEM micrographs showing characteristic microstructural elements produced after relatively low strains: (a) secondary twinning (true strain of 0.16), (b) multiply twinning (true strain of 0.16), (c) strain-induced transformation of twin (true strain of 0.16), (d) formation of dislocation boundaries (true strain of 0.16), (e) highly-developed substructure (true strain of ≈0.5), (f) poorly-developed substructure (true strain of ≈0.5).

flow stress and crystal rotations may activate additional (i.e., non-prism) slip modes. Indeed, the operation of pyramidal < c+a > slip was deduced from the analysis misorientation-axis distributions (Section 3.3.1). Because the pyramidal < c+a > slip mode includes 12 systems, its activation might provide a large increase in dislocation density. It was indeed observed in the present work (Fig. 8). In turn, the rapid increase in slip activity should enhance the occurrence of CDRX. Taken together with extensive mechanical twinning, this effect explains the formation of ultrafine grains even after true strains as low as only ~1.1 (Fig. 2c).

Considering the relatively high CRSS for pyramidal < c+a > slip, it is reasonable to assume that it would tend to occur preferentially in local, highly-stressed areas such as grain-boundary regions at which grain-to-grain interactions may also give rise to higher-than-average stresses. If so, this should lead to the nucleation of ultrafine grains in such areas and eventually result in necklace-type microstructures such as were observed herein (Fig. 2c–g).

Therefore, it was surmised that the specific character of CDRX observed in the present work was likely associated with the difficulty of activation of non-prism slip systems.

4.2. Effect of the change of the strain path

According to the widely accepted grain-subdivision model [39], the development of deformation-induced boundaries is governed by the diverging rotation of subgrains toward different crystallographic orientations, which are stable for specific modes of macroscopic deformation. Hence, grain refinement is closely linked with texture evolution. A change in strain path would promote the activation of new slip systems and may thus enhance the microstructural-refinement processes. In the present work, however, grain-refinement tended to stagnate after a true strain of ~2 (Fig. 3c, and 4b-c).

In this context, the pronounced material softening observed after each change of strain path (Fig. 1b) is of particular interest. This phenomenon is often attributed to the Bauschinger Effect, i.e., a rapid increase of mobile dislocations in pre-strained material due to re-organization of dislocation boundaries. Considering the purely-dislocation nature of a significant fraction of the deformation-induced boundaries in the present work (Section 3.4.2), it is likely that they are not stable during the change in the strain path and may transform into arrays of free/mobile dislocations. This simple idea is

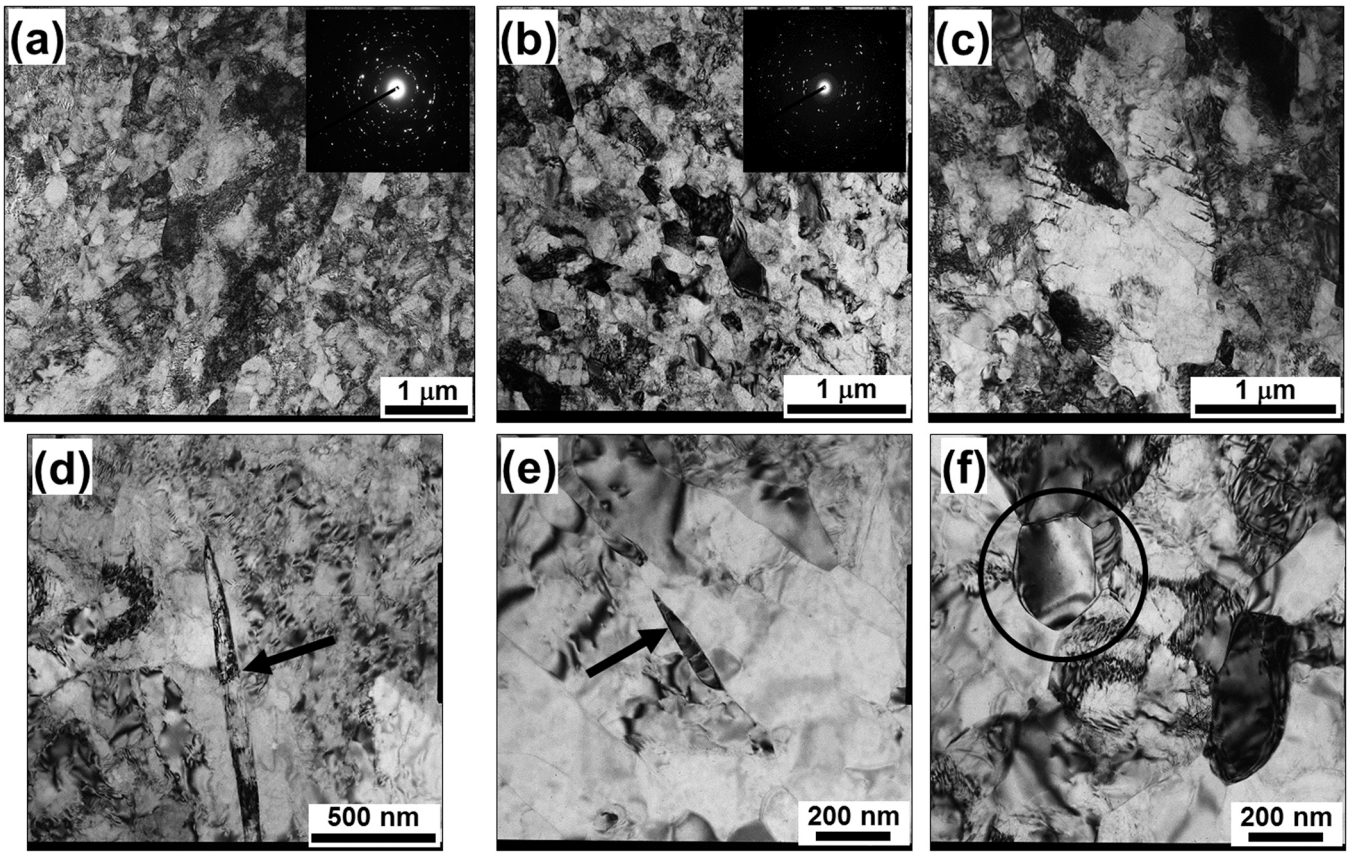

Fig. 7. TEM micrographs showing characteristic microstructural elements produced after relatively large strains: (a, b) nearly-globular microstructure (true strains of ≈2.2 and ≈6.7, respectively), (c) coarse-grained remnant of original grain structure (true strain of ≈6.7), (d) twin remnant (true strains of ≈3.8), (e) freshly-nucleated twin (true strain of ≈6.7), (f) recovered microstructure (true strains of ≈3.8). Note: Selected area diffraction patterns are shown in the insets in the top right corners of Figures (a) and (b).

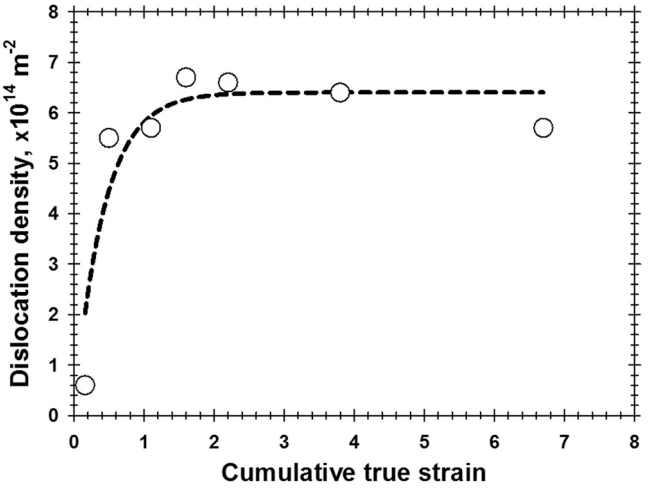

Fig. 8. Effect of cumulative strain on dislocation density.

in line with the development of a Luder's strain occasionally seen in stress vs strain diagrams (Fig. 1b), as well as the elimination of pre-existing dislocation structures after changes in strain path.

It is therefore suggested that the observed microstructural stabilization is a result of the re-organization of deformation-induced boundaries during strain-path changes.

5. Summary and conclusions

In this work, microstructure evolution during "abc" deformation of CP titanium was investigated. To this end, the program material was subjected to 12 deformation passes (involving an ~40-pct. height reduction each) at 400 °C and a nominal strain rate of 10^{-3} s^{-1}. Deformation-induced microstructure changes were investigated using EBSD and TEM techniques. The main conclusions derived from this study are as follows.

(1) As for monotonic modes of deformation, grain refinement consists of a two-stage process involving mechanical twinning at relatively-low strains and continuous dynamic recrystallization (CDRX) in the high-strain range. However, the contribution of twinning to microstructure evolution appears to be relatively-small, and the formation of a bulk UFG structure is primarily governed by CDRX.

(2) CDRX initiates preferentially at original grain boundaries or within twins. This occurrence results in an inhomogeneous, necklace-type microstructure. This unusual behavior can be attributed to the relatively-high local stresses in these areas, which should promote the activation of pyramidal < c+a > slip, and thus enhance the progressive development of dislocation boundaries.

(3) A change in strain path results in material softening, i.e., a phenomenon reminiscent of the Bauschinger Effect. Hence, it appears that strain-path changes can give rise to the re-organization of pre-existing dislocation structures and thus retard the progressive evolution of dislocation boundaries. In turn, this suppresses grain refinement.

CRediT authorship contribution statement

S. Mironov: Data curation, Formal analysis, Investigation, Methodology, Software, Validation, Visualization, Writing – original draft. **S. Zherebtsov:** Conceptualization, Investigation, Funding acquisition, Project administration, Supervision, Writing – review & editing. **S.L. Semiatin:** Conceptualization, Writing – review & editing.

Data Availability

The raw/processed data required to reproduce these findings cannot be shared at this time as the data also forms part of an ongoing study.

Declaration of Competing Interest

The authors declare that they have no known competing financial interests or personal relationships that could have appeared to influence the work reported in this paper.

Acknowledgments

The authors are also would like to thank the personnel of the Joint Research Center "Technology and Materials" at Belgorod State National Research University and Dr. G. Dyakonov for experimental assistance.

Appendix A. Supporting information

Supplementary data associated with this article can be found in the online version at doi:10.1016/j.jallcom.2022.165281.

References

[1] F.H. Froes, M. Qian (Eds.), Titanium in Medical and Dental Applications, Woodhead Publishing, Duxford, United Kingdom, 2018(654p; eBook ISBN: 9780128124574).
[2] R.Z. Valiev, Y. Estrin, Z. Horita, T.G. Langdon, M.J. Zehetbauer, Y. Zhu, Producing bulk ultrafine-grained materials by severe plastic deformation: ten years later, JOM 51 (2016) 7–18, https://doi.org/10.1007/s11837-016-1820-6
[3] R. Valiev, Nanostructuring of metals by severe plastic deformation for advanced properties, Nat. Mater. 8 (2004) 511–516, https://doi.org/10.1038/nmat1180
[4] R.Z. Valiev, T.G. Langdon, Achieving exceptional grain refinement through severe plastic deformation: new approaches for improving the processing technology, Metall. Mater. Trans. 42A (2011) 2942–2951, https://doi.org/10.1007/s11661-010-0556-0
[5] H. Miura, M. Kobayashi, T. Aoba, H. Aoyama, T. Benjanarasuth, An approach for room-temperature multi-directional forging of pure titanium for strengthening, Mater. Sci. Eng. A731 (2018) 603–608, https://doi.org/10.1016/j.msea.2018.06.060
[6] Z. Bézi, G. Krállics, M. El-Tahawy, P. Pekker, J. Gubicza, Processing of ultrafine-grained titanium with high strength and good ductility by a combination of multiple forging and rolling, Mater. Sci. Eng. A688 (2017) 210–217, https://doi.org/10.1016/j.msea.2017.01.112
[7] S.Yu Mironov, G.A. Salishchev, M.M. Myshlyaev, R. Pippan, Evolution of misorientation distribution during warm 'abc' forging of commercial-purity titanium, Mater. Sci. Eng. A418 (2006) 257–267, https://doi.org/10.1016/j.msea.2005.11.026
[8] G.A. Salishchev, R.M. Galeev, S.P. Malysheva, S.V. Zherebtsov, S.Yu Mironov, O.R. Valiakhmetov, E.I. Ivanisenko, Formation of submicrocrystalline structure in titanium and titanium alloys and their mechanical properties, Met. Sci. Heat Treat. 48 (2006) 63–69, https://doi.org/10.1007/s11041-006-0045-7
[9] G.A. Salishchev, S.Yu Mironov, S.V. Zherebtsov, Mechanism of submicrocrystalline structure formation in titanium and two-phase titanium alloy during warm severe processing, Rev. Adv. Mater. Sci. 11 (2006) 152–158.
[10] Y.P. Sharkeev, A.Y. Eroshenko, V.I. Danilov, A.I. Tolmachev, P.V. Uvarkin, Yu.A. Abzaev, Microstructure and mechanical properties of nanostructured and ultrafine-grained titanium and the zirconium formed by the method of severe plastic deformation, Russ. Phys. J. 56 (2014) 1156–1162, https://doi.org/10.1007/s11182-014-0156-3
[11] G.A. Salishchev, S.V. Zherebtsov, O.R. Valiakhmetov, R.M. Galeyev, S. Yu, Mironov, *Development of submicrostructalline titanium alloys using "abc" isothermal forging*, Mater. Sci. Forum 447–448 (2004) 459–464.
[12] S.V. Zherebtsov, S.Yu Mironov, G.A. Salishchev, Submicrostructaline structure formation in Ti and Ti-6Al-4V alloy by warm "abc" deformation, Mater. Sci. Forum 551–552 (2007) 183–188.
[13] S.P. Malysheva, G.A. Salishchev, S.Yu Mironov, S.Ya Betsofen, Grain growth and texture evolution during annealing of submicrocrystalline titanium produced by severe plastic deformation, Mater. Sci. Forum 467–470 (2004) 1289–1294.
[14] S. Zherebtsov, E. Kudryavtsev, G. Salishchev, Mechanism of microstructure refinement in titanium during "abc" deformation at 400°C, Mater. Sci. Forum 667–669 (2011) 439–444.
[15] S.V. Zherebtsov, Efficiency of the strengthening of titanium and titanium alloys of various classes by the formation of an ultrafine-grained structure via severe plastic deformation, Russ. Metall. (2012) 969–974, https://doi.org/10.1134/S0036029512110146
[16] D.K. Chouhan, S. Biswas, A.K. Singh, A.J. Shukla, High tensile strength-ductility combination in cold multiaxial plane-strain forged and rolled nanostructured titanium, Materialia 11 (2020) 100698, https://doi.org/10.1016/j.mtla.2020.100698
[17] D.K. Chouhan, S. Biswas, Multiaxial plane-strain forging and rolling of biomedical grade titanium: evolution of microstructure, texture, and mechanical properties, Mater. Lett. 291 (2021) 129540, https://doi.org/10.1016/j.matlet.2021.129540
[18] I. Ansarian, M.H. Shaeri, M. Ebrahimi, P. Minárik, K. Bartha, Microstructure evolution and mechanical behaviour of severely deformed pure titanium through multi directional forging, J. Alloy Compd. 776 (2019) 83–95, https://doi.org/10.1016/j.jallcom.2018.10.196
[19] B. Wang, X. Wang, J. Li, Formation and microstructure of ultrafine-grained titanium processed by multi-directional forging, J. Mater. Eng. Perform. 25 (2016) 2521–2527, https://doi.org/10.1007/s11665-016-2079-3
[20] P.C. Zhao, G.J. Yuan, R.Z. Wang, B. Guan, Y.F. Jia, X.C. Zhang, S.T. Tu, Grain-refining and strengthening mechanisms of bulk ultrafine grained CP-Ti processed by L-ECAP and MDF, J. Mater. Sci. Technol. 83 (2021) 196–207, https://doi.org/10.1016/j.jmst.2021.01.019
[21] S. Yamamoto, Y. Miyajima, C. Watanabe, R. Monzen, T. Tsuru, H. Miura, Dependences of grain size and strain rate on deformation behavior of commercial purity titanium processed by multidirectional forging, Mater. Trans. 61 (2020) 2320–2328, https://doi.org/10.2320/matertrans.MT-M2020263
[22] V. Danilov, A. Eroshenko, Y. Sharkeev, D. Orlova, L. Zuev, Titanium and zirconium base alloys in ultra-fine grain state: mechanical stability and failure behavior, Key Eng. Mater. 683 (2016) 162–167, https://doi.org/10.4028/www.scientific.net/KEM.683.162
[23] P. Yu, A. Sharkeev, V.I. Yu. Eroshenko, I.A. Danilov, A.I. Glukhov, Tolmachev, Production of ultrafine-grain bioinert alloys, Steel Transl. 45 (2015) 116–119, https://doi.org/10.3103/S096709121502014X
[24] S. Zherebtsov, E. Kudryavtsev, G. Salishchev, Mechanisms of microstructure refinement in titanium during "abc" deformation at 400°C, Mater. Sci. Forum 667–669 (2011) 439–444, https://doi.org/10.4028/www.scientific.net/MSF.667-669.439
[25] S.V. Zherebtsov, S.Yu Mironov, G.A. Salishchev, Submicrocrystalline structure formation in Ti and Ti-64 alloy by warm "abc" deformation, Mater. Sci. Forum 551–552 (2007) 183–188.
[26] G.A. Salishchev, S.Yu Mironov, S.V. Zherebtsov, Mechanisms of submicrocrystalline structure formation in titanium and two-phase titanium alloy during warm severe processing, Rev. Adv. Mater. Sci. 11 (2006) 152–158.
[27] S.P. Malysheva, G.A. Salishchev, S.Y. Mironov, S.Y. Betsofen, Grain growth and texture evolution upon annealing of a submicrocrystalline titanium obtained by severe plastic deformation, Phys. Metal. Metallogr. 99 (2005) 66–72.
[28] G.A. Salishchev, S.V. Zherebtsov, O.R. Valiakhmetov, R.M. Galeyev, S. Yu, Mironov, *Development of submicrocrystalline titanium alloys using "abc" isothermal forging*, Mater. Sci. Forum 447–448 (2004) 459–464.
[29] S.P. Malysheva, G.A. Salishchev, S.Yu Mironov, S.Ya Betsofen, Grain growth and texture evolution during annealing of submicrocrystalline titanium produced by severe plastic deformation, Mater. Sci. Forum 467–470 (2004) 1289–1294.
[30] B. Wang, J. Li, J. Sun, X. Wang, Z. Liu, Shear localization and its related microstructural evolution in the ultrafine grained titanium processed by multi-axial compression, Mater. Sci. Eng. A 612 (2014) 227–235, https://doi.org/10.1016/j.msea.2014.06.042
[31] Y. Ito, N. Hoshi, T. Hayakawa, C. Ohkubo, H. Miura, K. Kimoto, Mechanical properties and biological responses of ultrafine-grained pure titanium fabricated by multi-directional forging, Mater. Sci. Eng. B 245 (2019) 30–36, https://doi.org/10.1016/j.mseb.2019.05.002
[32] I. Ansarian, M.H. Shaeri, M. Ebrahimi, P. Minarik, K. Bartha, Microstructure evolution and mechanical behaviour of severely deformed pure titanium through multi directional forging, J. Alloy Compd. 776 (2019) 83–95, https://doi.org/10.1016/j.jallcom.2018.10.196
[33] G. Salishchev, S. Mironov, S. Zherebtsov, A. Belyakov, Changes in misorientations of grain boundaries in titanium during deformation, Mater. Character 61 (2010) 732–739, https://doi.org/10.1016/j.matchar.2010.04.005
[34] H. Conrad, Effect of interstitial solutes on the strength and ductility of titanium, Prog. Mater. Sci. 26 (1981) 123–403, https://doi.org/10.1016/0079-6425(81)90001-3
[35] F.J. Humphreys, Quantitative metallography by electron backscattered diffraction, J. Microsc. 195 (1999) 170–185, https://doi.org/10.1046/j.1365-2818.1999.00578.x
[36] Y. Huang, P.B. Prangnell, The effect of cryogenic temperature and change in deformation mode on the limiting grain size in a severely deformed dilute

aluminium alloy, Acta Mater. 56 (2008) 1619–1632, https://doi.org/10.1016/j.actamat.2007.12.017
[37] Y.B. Chun, S.H. Yu, S.L. Semiatin, S.K. Hwang, Effect of deformation twinning on microstructure and texture evolution during cold rolling of CP-titanium, Mater. Sci. Eng. A398 (2005) 209–219, https://doi.org/10.1016/j.msea.2005.03.019
[38] Y.B. Chun, M. Battaini, C.H.J. Davies, S.K. Hwang, Distribution characteristics of in-grain misorientation axes in cold-rolled commercially pure titanium and their correlation with active slip modes, Metall. Mater. Trans. A 41 (2010) 3473–3487, https://doi.org/10.1007/s11661-010-0410-4
[39] D.A. Hughes, N. Hansen, High angle boundaries formed by grain subdivision mechanism, Acta Mater. 45 (1997) 3871–3886, https://doi.org/10.1016/S1359-6454(97)00027-X
[40] S.V. Zherebtsov, G.G. Dyakonov, G.A. Salishchev, A.A. Salem, S.L. Semiatin, The influence of grain size on twinning and microstructure refinement during cold rolling of commercial-purity titanium, Metall. Mater. Trans. A 47 (2016) 5101–5113, https://doi.org/10.1007/s11661-016-3679-0
[41] S.V. Zherebtsov, G.S. Dyakonov, A.A. Salem, V.I. Sokolenko, G.A. Salishchev, S.L. Semiatin, Formation of nanostructures in commercial-purity titanium via cryorolling, Acta Mater. 61 (2013) 1167–1178, https://doi.org/10.1016/j.actamat.2013.10.026
[42] A.A. Salem, S.R. Kalidindi, R.D. Doherty, S.L. Semiatin, Strain hardening due to deformation twinning in α-titanium: mechanisms, Metall. Mater. Trans. A 37 (2006) 259–268, https://doi.org/10.1007/s11661-006-0171-2
[43] Z.S. Basinski, M.S. Szczerba, M. Niewczas, J.D. Embury, S.J. Basinski, The transformation of slip dislocations during twinning of copper-aluminum alloy crystals, La Rev. De. Metall. – CIT/ Sci. Genie Des. Mater. 94 (1997) 1037–1043.